Global Gyrokinetic Simulations of Toroidal Electron Temperature Gradient Driven Mode in Reversed Shear Tokamaks

Y. Idomura, S. Tokuda, Y. Kishimoto

Department of Fusion Plasma Research, Naka Fusion Research Establishment,
Japan Atomic Energy Research Institute, Naka, Ibaraki, 311-0193, Japan

E-mail address of main author: idomuray@fusion.naka.jaeri.go.jp

Abstract: Using a global gyrokinetic toroidal particle code, the toroidal electron temperature gradient driven (ETG) turbulence is studied in positive and reversed shear tokamaks. In the positive shear configuration, the ETG mode shows a ballooning structure, and its envelope width $\Delta r/\rho_{te}$, which is limited by a global ω^*_{te}-shearing effect, is proportional to $\rho^{*-1/2}$, where ω^*_{te} is the electron diamagnetic frequency and ρ^* is the electron Larmor radius ρ_{te} divided by the minor radius a. In the reversed shear configuration, the mode width of a slab like ETG mode, which is determined by a global magnetic field structure around the q_{min} surface, does not depend on ρ^*. According to the mixing length theory, a ballooning mode gives a Bohm like ρ^*-scaling, while a slab like mode shows a gyro-Bohm like ρ^*-scaling. In realistic small ρ^* tokamaks, the saturation level of the ETG mode in the positive shear configuration is order of magnitude higher than that in the reversd shear configuration. In the nolinear turbulent state, the ETG turbulence in the positive and reversed shear configurations show quite different structure formations. In the positive shear configuration, the ETG turbulence is dominated by streamers which have a ballooning type structure, and the electron temperature T_e profile is quickly relaxed to the maginally stable state in a turbulent time scale. In the reversed shear configuration, quasi-steady zonal flows are produced in the regative shear region, while the positive shear region is characterized by streamers. Accordingly, the electron thermal diffusivity χ_e has a gap structure across the q_{min} surface, and the T_e gradinet is sustained above the marginal value for a long time in the quasi-steady phase. The results suggest a stiffness of the T_e profile in positive shear tokamaks, and a possibility of the T_e transport barrier in reversed shear tokamaks.

1. Introduction

The electron temperature gradient driven (ETG) turbulence is considered as one of experimentally relevant electron transport mechanisms in tokamak plasmas [1,2]. In recent years, several gyrokinetic and gyrofluid simulations have provided substantial progress in understanding of the ETG turbulence. However, results from different simulation models contradict with each other in several respects. For example, local flux tube toroidal gyrokinetic simulations [3] showed extremely high electron heat conductivity χ_e in the moderate positive shear configuration, and it was explained by radially elongated structures or streamers. But, global toroidal [4] and local slab [5] gyrofluid simulations did not recover such a high χ_e. In the reversed shear configuration, global slab gyrokinetic simulations showed χ_e suppression by ETG driven zonal flows [6]. In order to comprehensively understand these qualitatively and quantitatively different results, the ETG turbulence in positive and reversed shear tokamaks with various machine size $\rho^{*-1}=200\sim10^5$ is investigated using a global gyrokinetic toroidal particle code GT3D [7], where ρ^* is the electron Larmor radius ρ_{te} divided by the minor radius a. In the annular (or full radius) wedge torus geometry, extremely high-n ETG modes (n>1000) are straightforwardly calculated using the quasi-ballooning representation. Although this treatment is similar to a local flux tube model, global profile effects are naturally retained. Especially, a global ω^*_{te}-shearing effect is important to determine the linear ballooning envelope width and the nonlinear streamer size, where ω^*_{te} is the electron diamagnetic frequency. Also, a global treatment of the q profile is essential to study reversed shear tokamaks. In this paper, we discuss difference between a global simulation and a local flux tube simulation with $\rho^*=0$ limit by showing ρ^*-dependence of the saturation level. Also, we show various structure formations in the ETG turbulence, and determine turbulent structures in the positive and reversed shear configurations.

2. Linear Stability Analysis and Mixing Length Theory

In this section, the linear stability of the toroidal ETG mode is analyzed in the positive and reversed shear configurations in Fig.1 (a). In the present analysis, plasma parameters are chosen based on the Cyclone base case [8] (deuterium, a circular concentric tokamak configuration, a/R_0=0.36, R_0/L_{ti}=R_0/L_{te}=6.92, R_0/L_n=2.22) except for the q profile. The density and temperature profiles are given in Fig.1 (b). The analysis domain is set around the reference magnetic surface r_0=0.5a where the density and temperature gradients peak.
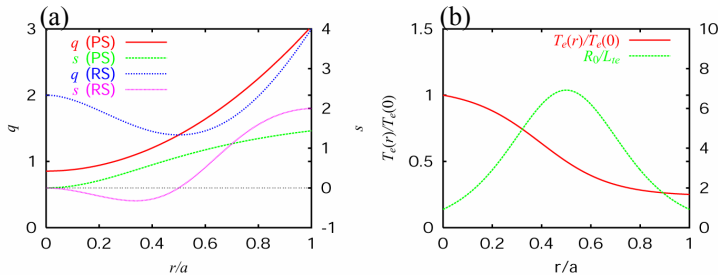

Fig.1: (a) shows the safety factor q(r) profile and the corresponding magnetic shear s=rq'/q. (b) shows the T_e(r) profile and its gradient parameter R_0/L_{te}. The critical value is R_0/L_{te}~4.5 (R_0/L_{te}~3.7) in the positive (reversed) shear configuration.
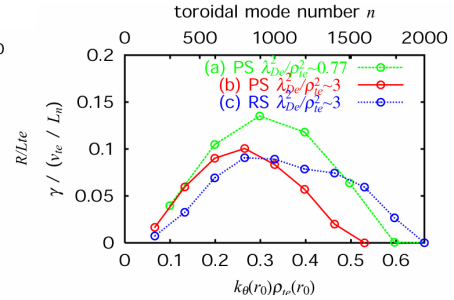
Fig.2: The growth rate spectrum of the ETG mode in positive and reversed shear tokamaks with a~8600ρ_{te} ~150ρ_{ti}.

2.1 Effects of Magnetic Configuration and Debye Shielding on Linear Growth Rate

Figure 2 shows the toroidal mode number n (or k_θ=nq_s/r) dependence of the growth rate γ spectrum in the positive and reversed shear configurations with experimentally relevant machine size a~8600ρ_{te}~150ρ_{ti}, where q_s is the safety factor defined in the straight-field-line coordinates. In the plot, three curves show the cases with (a) the positive shear configuration, $\lambda_{De}^2/\rho_{te}^2$~0.77 ($\beta$~0.02), (b) the positive shear configuration, $\lambda_{De}^2/\rho_{te}^2$~3 ($\beta$~0.005), and (c) the reversed shear configuration, $\lambda_{De}^2/\rho_{te}^2$~3 ($\beta$~0.005). Here, λ_{De} is the electron Debye length and β is the toroidal plasma beta. In the linear theory, the electrostatic electron/ion temperature gradient driven modes with adiabatic ions/electrons are isomorphic except for the Debye shielding effect. In our previous work [9], it was shown that in low density plasmas with $\lambda_{De}^2/\rho_{te}^2$>>1, the Debye shielding is effective and the unstable region of the ETG mode is characterized by $k_\theta\lambda_{De}$~1. In the high density case (a), the Debye shielding is not effective and the gyrokinetic Poisson equation is close to the quasi-neutrality condition. Therefore, the obtained spectrum agrees with the standard Cyclone benchmark result for the ITG mode [8] if the normalizations are replaced from v_{te} (ρ_{te}) to v_{ti} (ρ_{ti}). This shows a validity of the code in an extremely high-n regime. In the low density case (b), the Debye shielding effect becomes relatively important compared with the electron polarization effect. As a result, the growth rate becomes smaller and the peak of the spectrum shifts in the lower-n side. A comparison between the positive and reversed shear configurations can be seen by (b) and (c). According to the local ballooning analysis [10], the toroidal modes are stabilized as the magnetic shear changes from positive to negative. However, in the global analysis, the reversed-shear slab ETG modes [9] are excited in a weak magnetic shear region around the q_{min} surface. Because of this driving effect, the maximum growth rates are almost the same between (b) and (c).

2.2 ρ^*-dependence of Eigenmode Structure

Figure 3 shows poloidal harmonics of the linear eigenfunctions of the ETG modes in positive and reversed shear configurations with ρ^{*-1}=536/2146. In this ρ^* scan, the same equillibrium profiles are set as a function of r/a (Fig.1), and also the toroidal mode numbers n=50/200 are

chosen so that the normalized poloidal wavenumber becomes the most unstable value, $k_\theta\rho_{te}\sim0.3$. Thus, the calculations in Figs.3 (a) and (c) (Figs.3 (b) and (d)) are equivalent from a point of view of the local linear theory. In the positive shear case (Figs. 3 (a) and (c)), multiple poloidal harmonics are coupled to produce a typical ballooning structure. According to the higher order ballooning theory [11-13], the linear toroidal mode coupling is limited by a global ω^*_{te}-shearing effect, and the envelope width is estimated as $\Delta r \propto (\rho_{te}L_{te})^{1/2}$. If one assume $L_{te}\sim a$, the normalized envelope width is given by $\Delta r/\rho_{te} \propto \rho^{*-1/2}$. This dependence can be clearly seen in Figs.3 (a) and (c). In the case with $\rho^{*-1}=536$, the half envelope width is $\Delta r/\rho_{te}\sim60$, while $\Delta r/\rho_{te}\sim120$ in the case with $\rho^{*-1}=2146$. In the reversed shear case (Figs.3 (a) and (c)), the mode structure is quite different from the positive shear case. Although weak toroidal coupling structures can be seen in the positive shear region, the eigenfunction consists mainly of a few poloidal harmonics around the q_{min} surface. In the plot, in addition to a resonant mode with the poloidal mode number $m=m_0=nq_s$, nonresonant modes with $m=m_0-1,2...$ have large amplitudes. These nonresonant modes with a finite parallel wave number $k_{//}$ show a contribution from the reversed shear slab ETG mode. A mode structure of the reversed shear slab ETG mode is determined by the magnetic field structure around the q_{min} surface, and its mode width is given as $\Delta r/\rho_{te} \propto (L_{ns}/L_n)^{1/2}$ [9], where $L_{ns}=[2q(r_0)R_0/q''(r_0)r_0]^{1/2}$. Since L_{ns}/L_n is constant in the ρ^* scan, the mode width in Figs.3 (b), $\Delta r/\rho_{te}\sim45$, and (d), $\Delta r/\rho_{te}\sim40$, do not show a clear ρ^*-dependence.
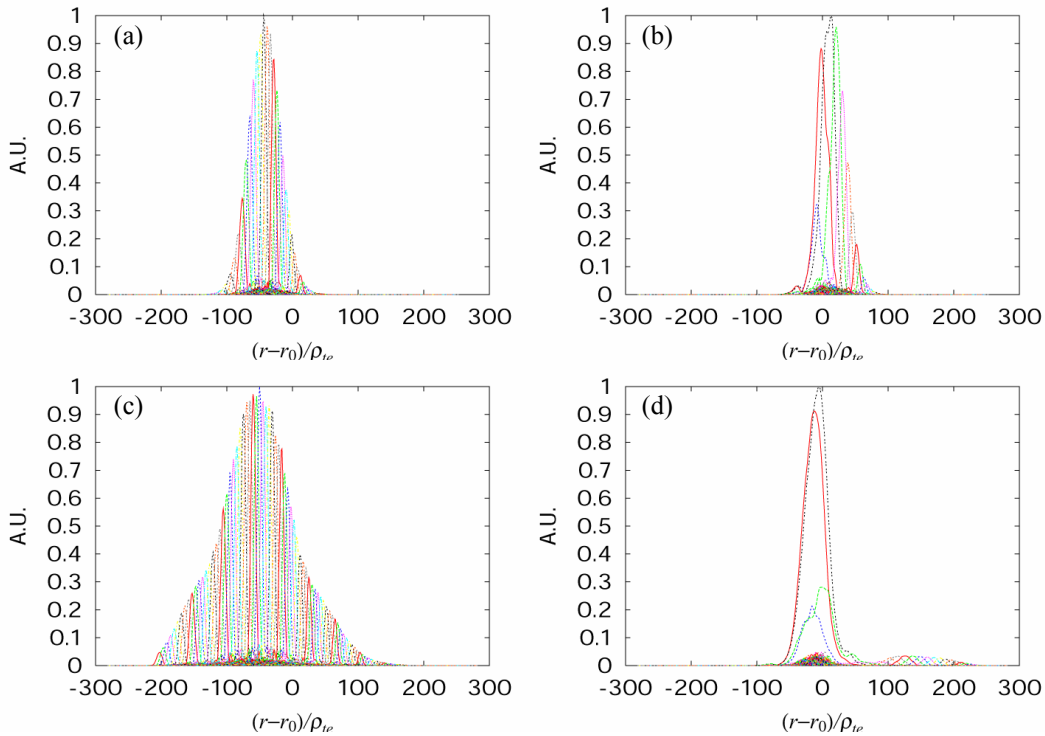

Fig.3: Plots of poloidal harmonics of the ETG mode in positive ((a), (c)) and reversed ((b), (d)) shear tokamks with $a=536\rho_{te}$ ((a), (b)) and $a=2146\rho_{te}$ ((c), (d)). The envelope width in the positive shear cases show a clear ρ^*-dependence. In the reversed shear cases, in addition to a resonant mode (black curve), non-resonant modes (red and blue curves) appear around the q_{min} surface $r=r_0$.

2.3 Single-n ETG Simulations and Mixing Length Theory

In the previous section, it is shown that in the positive shear configuration, $\Delta r/\rho_{te}$ of a ballooning mode is proportional to $\rho^{*-1/2}$, while in the reversed shear configuration, $\Delta r/\rho_{te}$ of a slab like mode does not have a clear ρ^*-dependence. From a point of view of the mixing length theory [14], where the thermal diffusivity is given by $\chi_e\sim\gamma\Delta r^2$, these features suggest different ρ^*-dependences of the saturation level. In order to clearly see this point, we show the

ρ^* scan of single-n nonlinear simulations by suppressing multiple-n nonlinear coupling. In this ρ^* scan, the normalized system size is chosen as $\rho^{*-1}=268\sim2146$, and, as in the previous section, the other parameters are chosen so that all the simulations become equivalent from a point of view of the local linear theory. Figures 4 (a) and (b) show the time history of χ_e/χ_{GB} averaged around $r=r_0$, where $\chi_{GB}=v_{te}\rho_{te}^2/L_{te}$. In the linear phase, the normalized growth rate $\gamma_n=\gamma/(v_{te}/L_{te})$ does not depend on ρ^* in all the cases in the positive and reversed shear configurations, respectively. However, in the positive shear configuration, the saturation levels are order of magnitude different depending on ρ^*, while in the reversed shear configuration, the saturation levels do not depend on ρ^*. It is noted that in the positive shear simulations, the temperature gradient is relaxed to the mariginaly stable state after the nonlinear saturation, and ,therefore, the dominant saturation mechanism is quasilinear flattening of the T_e profile. According to the mixing length theory, the saturation level in the positive shear configuration shows a Bohm like ρ^* scaling $\chi_e/\chi_{GB}\propto\gamma_n\rho^{*-1}$, while a gyro-Bohm like ρ^* scaling $\chi_e/\chi_{GB}\propto\gamma_n L_{ns}/L_n$ is expected in the positive shear configuration. This estimation is qualitatively consistent with the ρ^*-dependence of the saturation level in Fig.5. In the reversed shear configuration, the saturation levels are almost constant with $\chi_e/\chi_{GB}=1\sim2$. In contrast, in the positive shear configuration, the saturation level $\chi_e/\chi_{GB}=2\sim20$ drastically increase depending on ρ^*. This result may partly explain why flux tube gyrokinetic simulations [3], which correspond to $\rho^{*-1}=\infty$ limit, and the small size ($\rho^{*-1}\sim100$) global gyrofluid simulations [4] gave order of magnitude different transport levels.
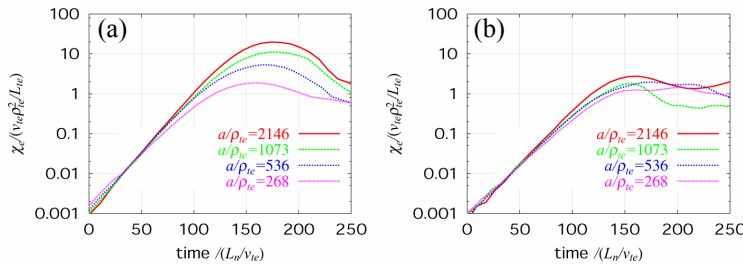

Fig.4:The time history of the averaged χ_e around $r=r_0$ in single-n nonlinear calculations in (a) positive and (b) reversed shear tokamaks.
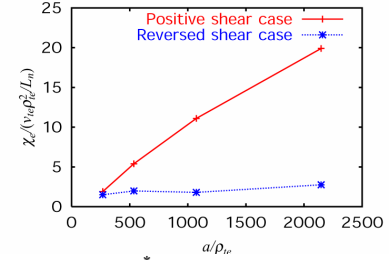
Fig.5:ρ^*-dependence of the saturation level in Fig.4.

3 Nonlinear Simulations of Toroidal ETG Modes

Although single-n simulations show clear correspondence between the mixing length theory and the ρ^*-scaling, the reality is much more complicated because of a multiple-n nonlinear mode coupling which leads to structure formations such as zonal flows and streamers. In order to address this issue, we perform multiple-n wedge torus simulations. Plasma parameters used in the simulation are same as in Sec. 2.1 ($a\sim8587\rho_{te}\sim152\rho_{ti}$). In the simulation, the size of the annular torus is chosen as $L_r=600\rho_{te}\sim1200\rho_{te}$, toroidal mode numbers are chosen as n=0, 100, 200...3100 in a 1/100 wedge torus section, and in the quasi-ballooning representation, the width of the poloidal mode number spectrum is determined to cover all the mode-rational surfaces in the simulation domain. In order to avoid effects from the boundary in a long time nonlinear simulation, we prepare linearly stable regions near the boundary. The conservation properties are improved by the optimized loading, and the breakdown of the total energy conservation is smaller than the saturation amplitude of the ETG mode even after the nonlinear saturation.

3.1 ETG Turbulence in Positive Shear Configuration

Figure 6 shows the time evolution of the electrostatic potential (in the bad curvature side $\theta\sim0$) of the ETG turbulence in the positive shear configuration. In the linear phase (Fig.6 (a)), a dominant mode with $k_\theta\rho_{te}\sim0.3$ shows a typical ballooning structure. In the initial saturation

phase, the background T_e profile is slightly relaxed by the heat transport, and a number of coupled poloidal harmonics increases to form large streamers which are expanded beyond the linear ballooning envelope width (Fig.6 (b)). In the initial saturation phase, the n-spectrum is dominated by a few n modes (Fig.7 (a)), and the saturation processes are very similar to single-n simulations in Sec. 2.3. This large quasi-linear streamer provides a very high saturation level $\chi_e/\chi_{GB}\sim10$ (Fig.7 (d)), and the T_e gradient is quickly relaxed from $R_0/L_{te}\sim7$ to $R_0/L_{te}\sim5$, which is close to the critical gradient $R_0/L_{te}\sim4.5$, in a turbulent time scale $\sim5\gamma^{-1}$. This high transport level, which is consistent with the previous flux tube simulations [3], suggests a stiffness of the T_e profile. It should be noted that because of adiabatic ion response on zonal flows, zonal flows are very weak in the initial saturation phase of the ETG mode. Therefore, in the ETG mode, a dominant saturation mechanism is a quasi-linear T_e flattening instead of
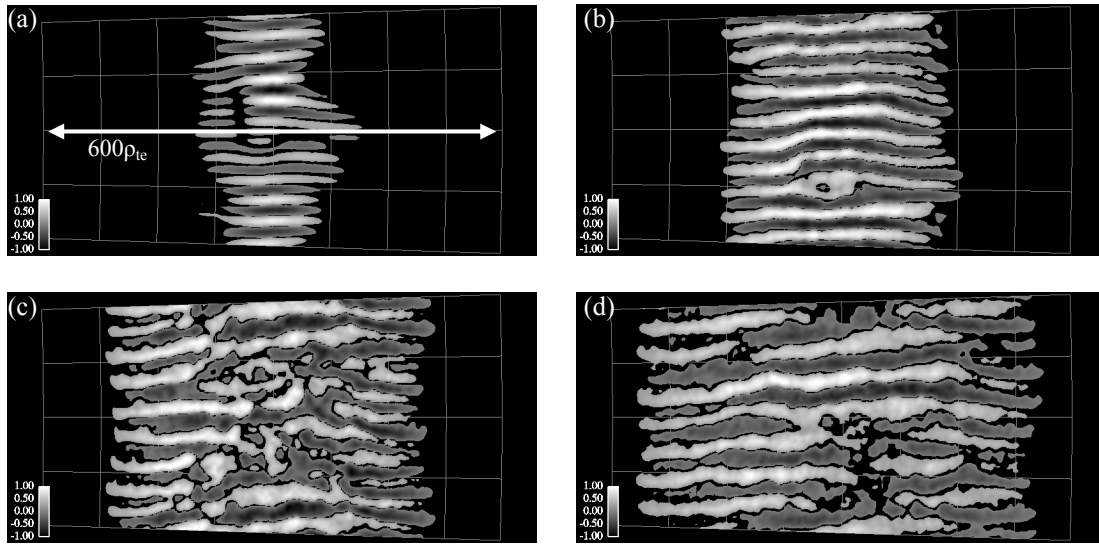

Fig.6: The electrostatic potential in the ETG turbulence simulations in the positive shear configuration. The plots show (a) linear phase ($t=110L_n/v_{te}$), (b) initial saturation phase ($t=175L_n/v_{te}$), (c) saturation phase ($t=208L_n/v_{te}$), and (d) quasi-steady phase ($t=250L_n/v_{te}$).
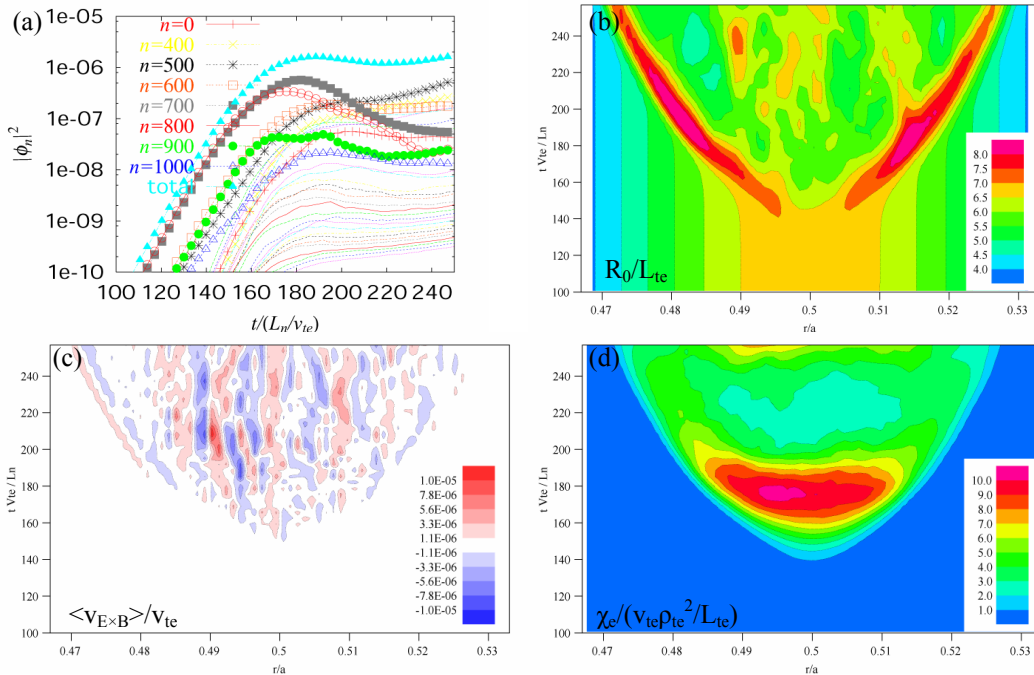

Fig.7: The time histories of (a) the n-spectrum, (b) the temperature gradient, (c) the electronthermal diffusivity, and (d) the flux surface averaged zonal flow amplitude in the ETG turbulence simulations in the positive shear configuration. In (b), the critical temperature gradient is $R_0/L_{te}\sim4.5$.

zonal flow suppression which is an important saturation mechanism of the ITG mode. After the nonlinear saturation, the turbulent region spreads in the radial direction through avalanche processes to propagate high R_0/L_{te} regions (Fig.7 (b)). Then, a low R_0/L_{te} region is formed between high R_0/L_{te} regions, and the initial streamer is broken up by the shearing of ω^*_{te} (Fig.6 (c)). This low R_0/L_{te} region continues to spread in time, and the second streamer with $k_\theta\rho_{te}\sim0.2$ is formed in the quasi-steady phase (Fig.6 (d)). In the positive shear configuration, the ETG turbulence is dominated by streamers which have a ballooning structure and oscillate with $\omega\sim\omega^*_{te}$, and quasi-steady zonal flows are not observed (Fig.7 (c)).

3.2 ETG Turbulence in Reversed Shear Configuration

In the reversed shear configuration, the nonlinear evolution of the toroidal ETG turbulence is very similar to that of the slab ETG turbulence [7]. In the linear phase (Fig.8 (a)), a slab like ETG mode with $k_\theta\rho_{te}\sim0.3$ is excited around the q_{min} surface. As in the positive shear case, the initial saturation phase is dominated by a few n modes (Fig.9 (a)). However, the linear mode width is smaller than the positive shear case, and a quasi-linear mode broadening is not observed. Accordingly, the saturation level is relatively lower $\chi_e/\chi_{GB}\sim5$, and the heat flux is localized around the q_{min} surface (Fig.9 (d)). After the nonlinear saturation, a weak shear region around the q_{min} surface is characterized by almost isotropic turbulent structures, and the turbulent region spreads almost symmetrically in both sides of the q_{min} surface by avalanche processes between the ETG mode and a formation of high R_0/L_{te} regions (Fig.8 (b)). However, in the nonlinear evolution phase, positive and negative shear regions show quite different features. In the negative shear region, secondary instabilities with $k_\theta\rho_{te}\sim0.25$ are excited (fig.8 (c)), and a corrugated density profile is formed. After the saturation of the secondary instability, quasi-steady zonal flows are sustained (Fig.9 (d)), and the ETG turbulence is regulated. It is noted that in the ETG turbulence, collisionless zonal flow damping is weak for $(k_r\rho_{te})^2\ll1$ [15]. On the other hand, in the positive shear region, large streamers with $k_\theta\rho_{te}\sim0.2$ are slowly formed (Fig.8 (d)). Since the equilibrium parameters in both regions are almost the same except for the magnetic shear, the positive magnetic shear, which drives a ballooning type toroidal coupling structures, is closely related to the streamer formation. In the quasi-steady phase, the χ_e distribution shows a clear gap structure across the q_{min} surface because of these qualitatively different turbulent structures in the positive and
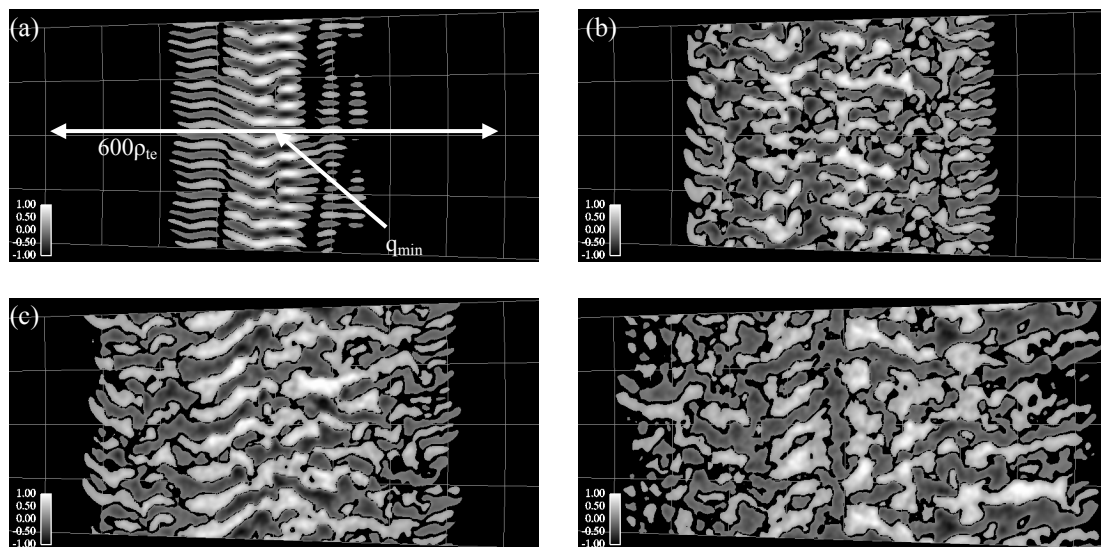

Fig.8: The electrostatic potential in the ETG turbulence simulations in the reversed shear configuration.
The plots show (a) linear phase ($t=110L_n/v_{te}$), (b) saturation phase ($t=207L_n/v_{te}$), (c) nonlinear evolution
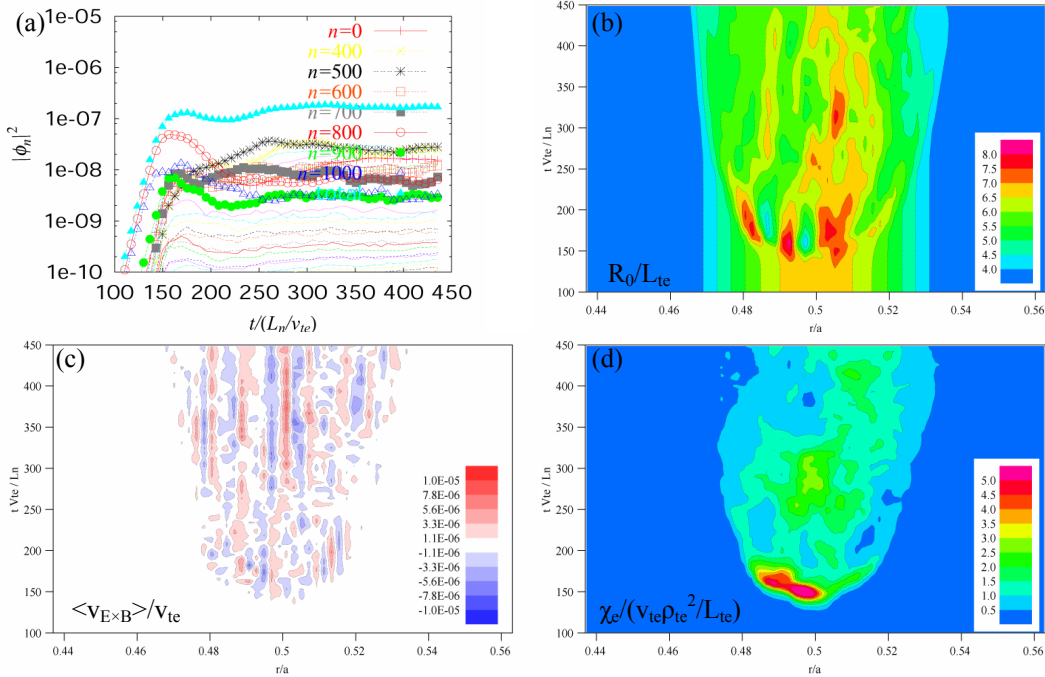*phase ($t=255L_n/v_{te}$), and (d) quasi-steady phase ($t=380L_n/v_{te}$).*

Fig.9: The time histories of (a) the n-spectrum, (b) the temperature gradient, (c) the electron heat conductivity, and (d) the flux surface averaged zonal flow amplitude in the ETG turbulence simulations in the reversed shear configuration. In (b), the critical temperature gradient is $R_0/L_{te} \sim 3.7$.

negative shear regions (Fig.9 (d)). In the reversed shear configuration, the temperature gradient is sustained above its critical value $R_0/L_{te} \sim 3.7$ for a long time in the quasi-steady phase (Fig.9 (b)), and this suggests a possibility of the T_e transport barrier.

4 Summary

Using a global gyrokinetic toroidal particle code GT3D, we have studied the ETG turbulence in positive and reversed shear tokamaks. In the positive shear configuration, the mode shows a typical ballooing structure, and it is confirmed that the ballooning envelope width $\Delta r/\rho_{te} \propto \rho^{*-1/2}$, which is limited by a global ω^*_{te}-shearing effect, shows a clear ρ^*-dependence. On the other hand, in the reversed shear configuration, the mode width of a slab like ETG mode $\Delta r/\rho_{te} \propto (L_{ns}/L_n)^{1/2}$, which is determined by a global q profile around the q_{min} surface, does not depend on ρ^*. According to the mixing length estimate, the former suggests a Bohm like ρ^*-scaling, while the latter suggests a gyro-Bohm like ρ^*-scaling. In single-n nonlinear simulations, these ρ^*-dependences of the saturation level are confirmed, and the saturation level in the small ρ^* positive shear configuration is order of magnitude higher than that in the reversed shear configuration and the large ρ^* positive shear configuration. Although multiple-n wedge torus simulations show much more complicated nonlinear behaviours, a tendency of the initial saturation level, which is dominated by a few n modes, is very similar to single-n simulations. Accordingly, in the positive shear configuration, the saturation level is order of magnitude higher than the reversed shear configuration, and the T_e profile is quickly relaxed to a marginally stable state in a turbulent time scale $\sim 5\gamma^{-1}$. In the nonlinear evolution phase, the ETG turbulence shows quite different structure formations in the positive and reversed shear configurations. The ETG turbulence in the positive shear configuration is dominated by large streamers, which have a ballooning type structure and oscillate with $\omega \sim \omega^*_{te}$. In the reversed shear configuration, quasi-steady zonal flows are produced in the negative shear region, while the positive shear region is characterized by streamers. This zonal flow generation is consistent with our previous global slab gyrokinetic simulations in reversed shear tokamaks [6]. Because of these qualitatively different structure formations in positive

and negative shear regions, the χ_e distribution shows a gap structure across the q_{min} surface, and the T_e gradient is sustained above its critical value for a long time in the quasi-steady phase. Within the framework of the collisionless toroidal ETG turbulence, the results suggest a stiffness of the T_e profile in the positive shear configuration, and a possibility of the T_e transport barrier in the reversed shear configuration. To discuss much more realistic electron heat transport, the gyrokinetic simulation of the ion temperature gradient driven-trapped electron mode [16] may also be important. A collisonal zonal flow damping [15] may affect on ETG driven zonal flows in the reversed shear configuration. These issues will be addressed in the future work.

References

[1]   HOANG, G.T., et al., "Experimental Determination of Critical Threshold in Electron Transport on Tore Supra", Phys. Rev. Lett. 87 (2001) 1250001-1.

[2]   STALLARD, B.W., et al., "Electron Heat Transport in Improved Confinement Discharges in DIII-D", Phys. Plasmas 6 (1999) 1978.

[3]   JENKO, F., et al., "Prediction of Significant Tokamak Turbulence at Electron Gyroradius Scales", Phys. Rev. Lett. 89 (2002) 225001-1.

[4]   LABIT, B., et al., "Global Numerical Study of Electron Temperature Gradient-driven Turbulence and Transport Scaling", Phys. Plasmas 10 (2003) 126.

[5]   LI, J., et al., "Numerical Study of Zonal Flow Dynamics and Electron Transport in Electron Temperature Gradient Driven Turbulence", Phys. Plasmas 11 (2004) 1493.

[6]   IDOMURA, Y., et al., "Stability of E×B Zonal Flow in Electron Temperature Gradient Driven Turbulence", Phys. Plasmas 7 (2000) 3551.

[7]   IDOMURA, Y., et al., "Global Gyrokinetic Simulation of Ion Temperature Gradient Driven Turbulence in Plasmas Using A Canonical Maxwellian Distribution", Nucl. Fusion 43 (2003) 234.

[8]   DIMITS, A.M., et al., "Comparisons and Physics Basis of Tokamak Transport Models and Turbulence Simulations", Phys. Plasmas 7 (2000) 969.

[9]   IDOMURA, Y., et al., "Gyrokinetic Theory of Slab Electron Temperature Gradient Mode in Negative Shear Tokamaks", Phys. Plasmas 7 (2000) 2456.

[10]   KIM, J.Y., et al., "Negative Shear Effect on Toroidal Ion Temperature Gradient Mode", Phys. Plasmas 2 (1995) 1012.

[11]   CONNER, J.W., "Shear Damping of Drift Waves in Toroidal Plasmas", Phys. Rev. Lett. 70 (1993) 1803.

[12]   KIM, J.Y., et al., "Radial Structure of High-Mode-Number Toroidal Modes in General Equilibrium Profiles", Phys. Rev. Lett. 73 (1994) 2200.

[13]   KISHIMOTO, Y., et al., "Toroidal Mode Structure in Weak and Reversed Magnetic Shear Plasmas and Its Role in The Internal Transport Barrier", Plasma Phys. Controlled Fusion 41(1999) A663.

[14]   KADOMTSEV, B.B., "Plasma Turbulence" (Academic Press, London 1965).

[15]   KIM, E., et al., "Collisional Damping of ETG-Mode-Driven Zonal Flows", Phys. Rev. Lett. 91 (2003) 075003-1.

[16]   IDOMURA, Y., et al., "Gyrokinetic Simulations of Tokamak Micro-Turbulence including Kinetic Electron Effects", 13th International Toki Conference, Toki, Japan (2003).